

River discharge monitoring using satellite missions: Sentinel-1, Sentinel-2, and Sentinel-3 (Case study: The Karun River, Iran)

Arash Tayfehrostami^{1*}, Alireza A. Ardalan¹, Amir Hossein Pourmina¹

¹School of Surveying and Geospatial Engineering, College of Engineering, University of Tehran, P.O. Box 11155-4563, Tehran, Iran.

Article history:

Received: 6 April 2020, Received in revised form: 18 August 2021, Accepted: 25 August 2021

ABSTRACT

With a length of 950 km, Karun River is the longest river in Iran. In this study, we aimed at application of Sentinel-3B satellite altimetry data as well as Sentinel-1 and Sentinel-2 satellite imagery for the estimation of Karun River discharge and validation with the in-situ data. Knowing that Level-2 altimetry data are not reliable for rivers and shallow waters, we opted to re-track the waveforms of Level-1B Sentinel-3B mission data and to test several re-tracking techniques for this purpose. The results showed that the threshold algorithm, with threshold of 90%, improves the accuracy of the time series of water level by 7.05% and increases the correlation with the in-situ gauge data by 12.7% as compared with those obtained via Level-2 data based on OCOG that was identified as the optimum re-tracker in this case. Next, from the estimated time series of the river's water level, the time series of Karun River discharge were evaluated in order to constitute our discharge estimation based on Sentinel-3B satellite altimetry data, which further to be compared with the discharge that we calculated using satellite imagery of Sentinel-1 and Sentinel-2, while taking the in-situ data as the benchmark. The river's discharge time series obtained from the altimetry data resulted in RMSE value of 852.31 m³/s, NSE coefficient of 0.19 m³/s, and correlation of 62.40% with the in-situ river discharge time series. On the other hand, the river discharge time series obtained from satellite imagery of Sentinel-1 mission resulted in RMSE value of 165.06 m³/s, NSE coefficient of 0.94 m³/s, and correlation of 97.12%, and Sentinel-2 mission the RMSE value 264.23 m³/s, NSE coefficient of 0.81 m³/s, and the correlation of 97.32% with in-situ data. The overall results of this study indicates that various Copernicus satellites missions have good potentiality for Karun River discharge monitoring.

KEYWORDS

Karun River
Retracking
Returned waveforms
Satellite radar altimetry
Satellite Imagery.

1. Introduction

Rivers are complex systems of natural water flows that flow in channels that play a crucial part in the water cycle and serve as the primary source of water supply. The mechanism for transporting surface runoff to water areas is significant for people's life and ecosystems. The size of rivers is classified according to discharge, drainage range, and river width. According to this classification, rivers with a width of 40 to 200 meters are small rivers, and rivers with a width of 200 to 800 meters and 800 to 1500 meters are defined as medium and large rivers, respectively. Components of river systems are an essential part of the hydrological cycle that connects land and ocean reservoirs.

However, many small and medium-sized rivers have few or no in situ gauge stations (Kebede et al., 2020).

A key parameter in river monitoring is the discharge, which its variations is directly related to the changes in the river's water level. River discharge is one of the fundamental climate variables in the water cycle, indicating changes and regulating the climate system. Although the need for river discharge information for various applications related to water resources management is well established, many basins still lack in-situ gauge stations, and surprisingly, the number of in-situ gauge stations at many basins around glob are decreasing, for various reasons (Calmant & Seyler, 2006; Feng et al., 2019; Gleason et al.,

* Corresponding author

E-mail addresses: ar.tayfehrostami@ut.ac.ir (Arash Tayfehrostami); ardalan@ut.ac.ir (Alireza A. Ardalan); pourmina@ut.ac.ir (A. Pourmina)

DOI: 10.22059/eoge.2022.336941.1112

2018; Gleason & Hamdan, 2017; Hossain et al., 2014; Sneeuw et al., 2014; Tarpanelli et al., 2013; Tourian et al., 2017; Di Baldassarre & Uhlenbrook, 2012).

The scarcity and sometimes nonexistence of discharge measurements, strongly affects the water resources management. For these reasons remote sensing within the past decades has become vital source of information to obtain water level and discharge, which are needed for efficient monitoring of water resources (Sulistioadi et al., 2015; W. Sun et al., 2012; W. C. Sun et al., 2010; Tang et al., 2009; Wang et al., 2019). Advances in technology, knowledge and economic capital have led to significant growth in effective and efficient monitoring of water resources and the creation of databases of lakes, reservoirs, and rivers (H. Gao, 2015; H. Gao et al., 2012; Sichangi et al., 2016), however, no due attention has been paid to the monitoring of small rivers (Sulistioadi et al., 2015). Therefore, special attention is necessary to the study of space-based discharge estimation of small and medium rivers, which are mostly the headwater of large rivers. The appropriate method of estimating the discharge based on remote sensing always depends on the accuracy of the estimated parameters obtained directly (width, slope, water level) or indirectly (acceleration and depth) from different satellite sensors and measuring techniques for these multiple hydraulic variables.

The main satellite sensors used to recover river discharge are optical, and radar imaging sensors that are used to measure river width (Smith & Pavelsky, 2008) and water velocity (Beltaos & Kääh, 2014; Tarpanelli et al., 2015) as well as radar altimeters, which provide the measure of river water level (Tourian et al., 2013; Zakharova et al., 2006). Through statistical relationships or hydraulic equations, these observations may be converted to river discharge. Reduction in the number of in-situ observations used to calibrate and validate hydrological models has led to satellite-model-dependent techniques (Biancamaria et al., 2009; Domeneghetti et al., 2014; Emery et al., 2018; Getirana & Peters-Lidard, 2013).

The use of altimetry observations to estimate river discharges began with the world's major rivers, such as the Ob River (Kouraev et al., 2004), the Amazon (Zakharova et al., 2006), the Brahmaputra, and the Ganges Delta (Frappart et al., 2010). Due to the improved accuracy of water level recovery in new altimeter missions, more rivers with smaller sizes and challenging geomorphology have become the focus of studies. As a general rule, smaller the rivers with more significant variability in their water regime, the shorter duration of flood events, and the more complex and irregular river geomorphology. These factors are essential for the water levels obtained from altimetry and the accuracy of the discharge from the conversion of the water level obtained from altimetry. Primary method for estimating discharge from satellite images and remote

sensing observations is based on establishing statistical relationships, rating curves (RC), between in-situ observations at the nearest in-situ gauge station, and water levels from altimetry (Kouraev et al., 2004; Tarpanelli et al., 2013) or hydraulic equations, and its estimated parameters (width, slope, height) (Gleason et al., 2014; LeFavour & Alsdorf, 2005).

Several studies have been performed using Sentinel-3 mission altimetry data for rivers; for example, seven altimetry mission data from 1995 to 2017 for Ogooué river have been studied to measure the water level, and the results showed that Sentinel-3 has less than 0.41m RMSE when considering the in-situ data as the benchmark (Bogning et al., 2018). The Brahmaputra River was studied using Sentinel-3A altimetry data, which resulted in a standard deviation of 0.41 to 0.76m compared to in-situ water levels (Huang et al., 2019). The Ebro River Basin was also studied using Sentinel-3 data, and the results showed good agreement with in-situ measurements within the RMSE of 0.28m (Q. Gao et al., 2019). Recently, in another study, the water level of Doroudzan Dam in Iran was monitored using level-2 and level-1B data of the Sentinel-3A mission. The results show the proper performance of the Sentinel-3 mission in monitoring small inland water bodies (Tayfeh Rostami et al., 2021).

In contrast with previous studies which have been conducted on relatively large rivers, this study aims at applying Sentinel-3 altimetry data and Sentinel-1 and Sentinel-2 satellite imagery to the Karun River, whose width varies from 208 to 373 meters, and to validate the derived discharges from these satellite missions with in-situ data. The main objectives of this study are as follows: (1) Estimation of water level from level-2 Sentinel-3B SRAL and its different re-trackers as well as and re-tracking of the returned waveforms of level-1B data of the same satellite, and then comparison with the in-situ water level gauges data to obtain the optimum satellite-derived water level and use it to estimate river discharge to be further compared with in-situ river discharge. (2) Calculating the river's width based on Sentinel-1 and Sentinel-2 images and then converting the calculated width to the river discharge and comparing with in-situ river discharge. (3) Comparison of the aforementioned satellite-based techniques for river discharge and finally, judgment on applicability of Copernicus satellite missions for water discharge monitoring of medium to small size rivers.

2. Study Area

Karun River, as the longest river in Iran, flowing from northeast to southwest of Khuzestan province. Karun catchment with an area of 68481 km² is bounded in the geographical latitude 30°17' - 33°49' and longitude 48°15' - 52°30', of which 23260 km² belong to the Dez basin, and 45221 km² belong to Karun basin. This basin is one of the

most frequently used watersheds in Iran. Its path provides drinking water, water for agriculture and industry in 16 cities and tens of villages and thousands of agricultural lands, hydropower generation, fish farming projects. Karun River consists of four main tributaries of Khorasan, Ab-e-Vanak, Ab-e-Kiar, and Bazaft. It originates from different heights, such as the northern heights of Ardakan Fars and

the south and west of Borujen. This river in the north of Shushtar is divided into two tributaries that are next connected in the south of Shushtar. This is the most important branch of Karun, that joins Karun in the north of Ahvaz. Upon entering Ahvaz, the Karun River divides the city into eastern and western parts, and most of the city's drinking water is supplied through the Karun River.

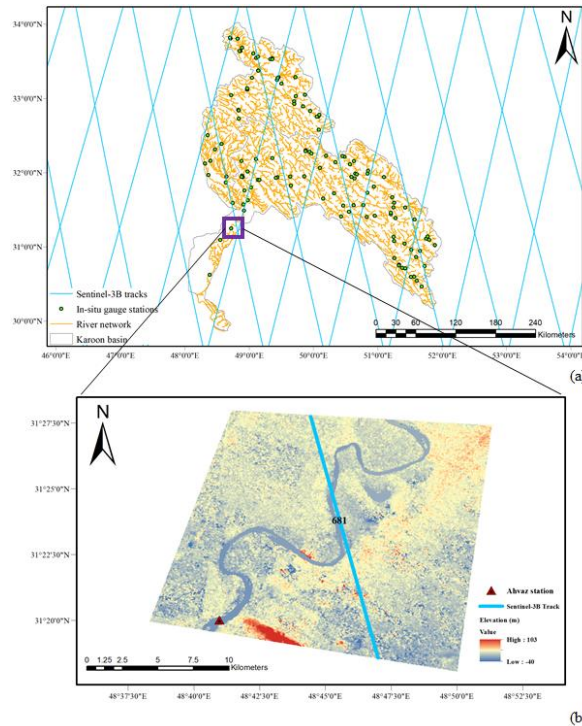


Figure 1. The Karun River basin: (a) Sentinel-3B satellite tracks cover the water bodies with all available gauging stations of the basin; and (b) Location of Ahwaz station and the pass number 681 of Sentinel-3B mission over Karun River with the elevation of the Karun River basin based on the digital elevation model from the shuttle radar topography mission.

3. In-situ and satellite dataset

3.1. In-situ gauge data

The Karun river's observed discharge and water level data in the Ahwaz station are taken from Khuzestan Water and Electricity Organization from January 2018 till May 2020 and were used to develop a hydraulic relationship (rating curve) to determine unknown parameters in discharge estimation as well as validation of models. Due to the river's limited observed flow data at the Ahwaz gauge site and its interruptions, Sentinel-3 data were used only on those days when both Sentinel-3 and in-situ gauge data were available. This led to satellite images that had relatively better access to in-situ gauge data in those days, and explains why in the mentioned period, the evaluation of satellite data with in-situ gauge data has not been done in some months. Besides, due to the high temporal resolution of satellite imagery, an attempt was made to select the images that cover the in-situ gauge on those days. Likewise, Sentinel-3 altimeter data were not collected for the months that in-situ gauge data were not, available (particularly during the year 2020).

3.1. Satellite data

3.2.1. Sentinel-3B

Sentinel-3B mission following the Sentinel-3A mission launched on April 25, 2018, and its data are available from December 2018. The SRAL is one of its sensors that is used to measure the water level and, as such used in this study. For details on Sentinel-3B SRAL we refer to its handbook offered by the European Space Agency, and only provide some technical characteristics of this mission in Table 1. Among the existing passes of this mission over the Karun Basin, after some examination, we found that only the pass number 681 has the best coverage over Karun River, and therefore it was used for our study (<https://scihub.copernicus.eu/dhus/#/home>).

Three levels of processed altimeter data are available for the Sentinel-3 SRAL mission, which are called Level-0, Level-1, and Level-2 products. The main objective of Level-2 product of SAR data is to provide elementary re-tracked altimeter estimates for the oceans, coastal zones, ice sheets, and sea ice elevations (EUMETSAT, 2017). The re-tracking algorithms that are more suited to the mentioned

areas are “ocean re-tracking”, “OCOG re-tracking”, “ice sheet re-tracking”, “ice re-tracking”, and “sea ice re-tracking”. Among the above re-tracking algorithms, ice re-tracker results are not available for inland water bodies.

In our study, Level-1B non-time-critical (NTC) 20 Hz data were used for the water level retrieval by the threshold re-tracker. Furthermore, Sentinel-3 Level-2 Ocean, OCOG, Ice Sheet. and, Sea Ice data from ESA within the period from October 2018 till February 2020 were used for the comparison. It should also be noted that when using satellite altimetry for the study of rivers, we use only over river observation of a long track data. Therefore, spatial

resolution of the satellite mission makes no sense here, and it is only the size of the footprint of the altimetry observation which matters. That footprint for new generation of altimetry satellites such as CryoSat-2 and Sentinel-3 is significantly improved, and as such has made them more successful for higher accuracy observations near the coastlines and confined inland water bodies such as lakes and rivers. It is clear that if by chance a satellite track is in-line with the river, we get more observations than the case it crosses over the river. The latter was the case in our study.

Table1. Basic parameters of Sentinel-3 SAR Altimeter (SRAL) instrument (EUMETSAT, 2017).

| Parameter | Ku band | C band |
|------------------------------------|---------------------------|----------|
| Tracking modes | Closed-loop and open-loop | |
| Low-resolution mode (LRM) PRF | 1920 Hz | |
| Synthetic Aperture Radar (SAR) PRF | 18 kHz | |
| SAR along with track resolution | ~300 m | |
| Nominal gate | 44 | |
| Pulse length | 3.125 ns | |
| Waveform gates | 128 | |
| Repeat cycle | 27 days | |
| Frequency | 13.575 GHz | 5.41 GHz |
| Bandwidth | 350 MHz | 320 MHz |
| Antenna beam width | 1.28° | 3.40° |

3.2.2. Sentinel-1 A&B

The Sentinel-1 mission is the first mission designed by the ESA under the Copernicus program. The Sentinel-1A satellite was launched in April 2014, and its twin satellite, Sentinel-1B was launched in April 2016 with a 180-degree orbital difference. Sentinel-1 satellites provide C-Band (center frequency 5.405 GHz) images with both single and dual polarization. A single satellite repeat cycle is 12 days, whereas a six-day repeat pass observation can be achieved with the two missions (Nagler et al., 2016). For Sentinel-1 SAR images four acquisition modes, namely, strip map, interferometric wide swath, extra-wide swath, and wave,

can be achieved for different levels of processing (Cazals et al., 2016). In this study we used Level-1 ground range detected images, which belong to the IW mode with VV polarization produced by Sentinel-1 A&B (<https://search.asf.alaska.edu/#/>) from January 2018 to June 2020 over Karun River. Besides, since the Karun river's entire area is apparent in a single image, there was no need to form a mosaic. The Sentinel-1 images used in this study are listed in Table 2. The product data of Sentinel-1 SAR images has a swath width of 250 km at a resolution of 5×20 m in the along and across track directions, respectively. The imagery pixel size of the sensor on ground is 10 m (Torres et al., 2012).

Table2. Sentinel-1 images that were used in this study.

| | |
|------------------|--------------------------|
| Number of Images | 30 [A: 14 B: 16] |
| Study period | January 2018 – June 2020 |
| Level | 1 |
| Format | GRD |
| Mode | IW |
| Incidence angle | 30° - 46° |
| Resolution | 5×20 m |
| Swath width | 250 km |
| Orbit | Descending |
| Polarization | VV |

3.2.3. Sentinel-2 A&B

The Sentinel-2 mission includes twin satellites, the Sentinel-2A, and the Sentinel-2B. The Sentinel-2A

launched on June 23, 2015; subsequently, on March 7, 2017, the Sentinel-2B mission was launched. The Sentinel-2 mission imaging sensor is called MSI, and its images

contain 13 spectral bands. These spectral bands ranging from visible and near infrared (VNIR) to shortwave infrared (SWIR) wavelengths along a 290-km orbital swath. The spatial resolution of Sentinel-2 mission images is variable in 10, 20, and 60 meters, depending on the spectral bands (Drusch et al., 2012).

Pre-processing of all data obtained from the Sentinel-2 Mission MSI sensor is done systematically at three levels, namely, Level-0, Level-1, and Level-2A. The Level-1C product processing includes radiometric and geometric corrections, including ortho-rectification and spatial registration on a global reference system with sub-pixel accuracy (ESA, 2015). In this study we used Level-1C data from Sentinel-2 mission images with a cloud cover below 20% during the study time period (January 2018 – June 2020) and number (30) of Sentinel-1 mission images.

4. Methodology

4.1. Water level from satellite altimetry

A space-borne radar altimeter is a primary tool for monitoring the oceans, but it can also be used for inland water bodies, including lakes, dams and, rivers. The principle of altimetry can be found in (Roohi, 2017) with the application of geophysical and atmospheric corrections. In this study we first extracted altimetry data for 681 passes of the Sentinel-3B mission over the river. Then, corrections for the wet troposphere, dry troposphere, ionosphere, solid earth tide, geocentric pole tide, COG, and the geoid were applied. As the study's objective was to directly exploit official Sentinel-3B L1B data and compare it against Level-2 official products, the use of the corrections available in the Level-2 product was considered. The corrections and their ranges are listed in Table 3.

Table 3. Atmospheric and geophysical corrections were used in this study from the Sentinel-3B Level-2 product.

| Correction | Source | Variable in Level-2 product | Range of correction |
|-------------------------|--|------------------------------------|---------------------|
| Dry troposphere | ECMWF model (Boehm et al., 2008) | mod_dry_tropo_cor_meas_altitude_01 | 1.7 – 2.5 m |
| Wet troposphere | ECMWF model (Boehm et al. 2008) | mod_wet_tropo_cor_meas_altitude_01 | 0 – 50 cm |
| Ionosphere | GIM (Scharroo & Smith, 2010) | iono_cor_gim_01_ku | 6 – 12 cm |
| Solid earth tide | Cartwright model (Cartwright & Edden, 1973) | solid_earth_tide_01 | -30 – +30 cm |
| Geocentric pole tide | Historical pole location (Wahr, 1985) | pole_tide_01 | -2 – +2 cm |
| Center of Gravity (COG) | ESA (ESA, Sentinel-3 Alimetry Technical Guide) | cog_cor_01 | 55 cm |
| Geoid | EGM 2008 (Pavlis et al., 2012) | geoid_01 | Mean: 30.6 m |

In order to improve the altimeter range accuracy behind that of re-trackers in Level-2 data over inland water bodies, the waveform needs to be re-tracked precisely to locate accurately tracking point on the leading edge of the waveform (Deng & Featherstone, 2006). Among various re-trackers that are tested we found that the threshold re-tracker described in Section 4.2, can provide most accurately the tracking points on the land-contaminated waveforms over the Karun River. After re-tracking the returned waveforms with the threshold algorithm, the bias between the datums of the in-situ gauge and altimetry water levels is calculated. Next, the outliers in observations are removed by polynomial fitting at 95% confidence level. Finally, the time series of water level differences among level-2 data, that which obtained by re-tracking the Sentinel-3B waveforms, and in-situ gauge data are generated for the validation.

4.2. Threshold re-tracker

The threshold re-tracker was developed in 1997 with the primary purpose of measuring the height of ice sheets

(Davis, 1997). The main advantages of this algorithm are implementation simplicity and its internal accuracy in terms of repeatability (Davis, 1995). In this sense, repeatability refers to the stability of the re-tracking in the selection of the re-tracking point (Davis, 1997). The threshold re-tracker is normally considered with 10%, 20%, and 50% thresholds. It has come out that the 10% threshold results in the highest repeatability, and the 20% threshold is suitable for measurements over the ice sheets. To find the re-tracking gate, a linear interpolation is performed between adjacent samples at a position where the threshold value passes through the leading edge of the waveform. The following is the computational procedure.

1. Thermal noise (PN) is obtained by averaging the first five gates:

$$P_N = \frac{1}{5} \sum_{i=1}^5 P_i \quad (1)$$

2. The amplitude is then calculated from the following Equation:

$$A = \sqrt{\frac{\sum_{i=1+n_1}^{N-n_2} iP_i^4(t)}{\sum_{i=1+n_1}^{N-n_2} P_i^2(t)}} \quad (2)$$

where N is the total number of waveform gates, and $n_1 = n_2 = 4$ are the beginning and end gates of waveform removed to prevent signal interference error (aliasing).

3. The threshold level is obtained from the following Equation:

$$Th = P_N + q(A - P_N) \quad (3)$$

where A is calculated from Equation (2) and q is the threshold value (for example, 0.2 equals 20%).

4. The $Gate_{ret}$ is calculated from the following Equation:

$$Gate_{ret} = (k - 1) + \frac{Th - P_{k-1}}{P_k - P_{k-1}} \quad (4)$$

where k is the first gate whose power exceeds the threshold Th . Figure 2, shows the waveforms of pass 340 and cycle 35, and Figure 3 shows the re-tracked waveform of the same pass and cycle using the threshold re-tracker for 10% to 90% thresholds.

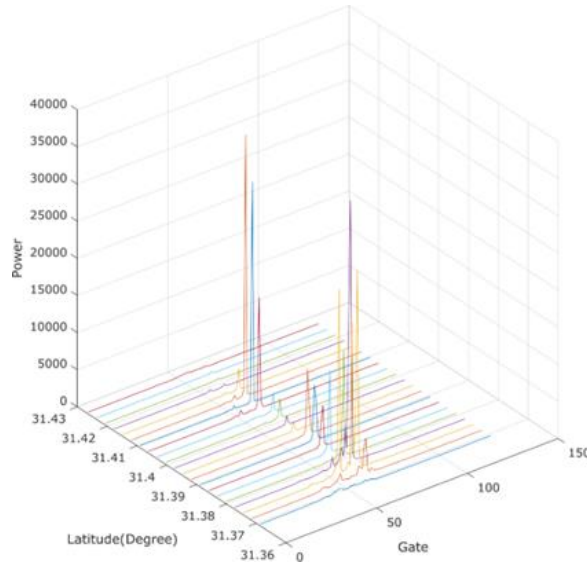


Figure 2. Waveforms of the pass 340 and cycle 35 of the Sentinel-3B mission on the Karun River.

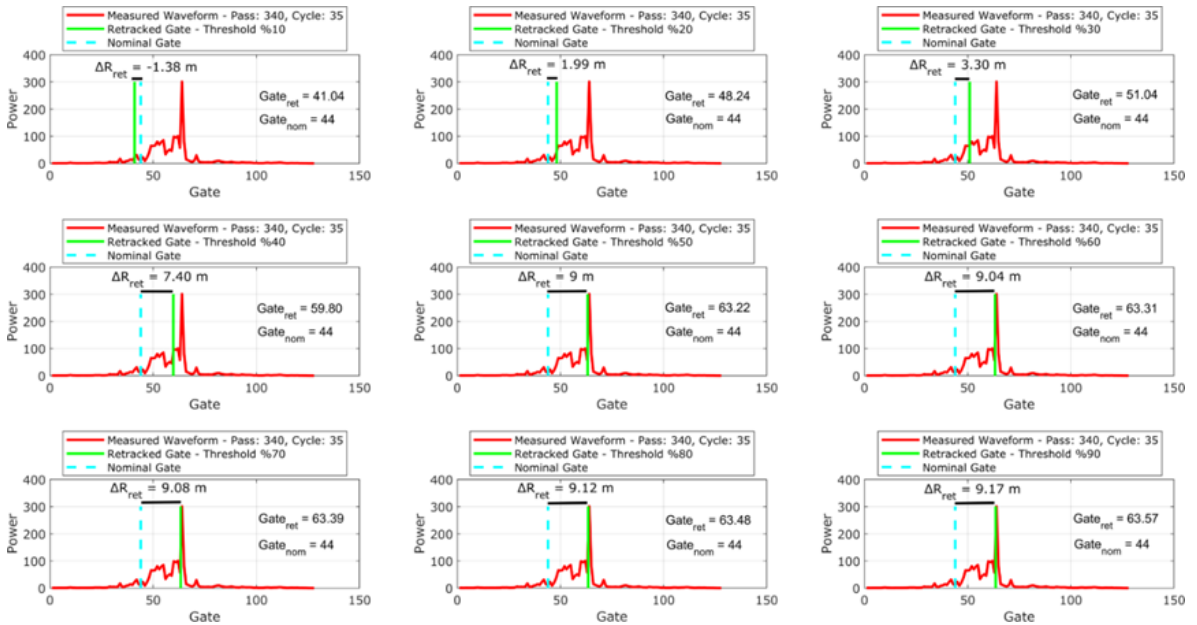


Figure 3. Re-tracked waveform of pass 340 and cycle 35 of Karun River in Ahwaz using threshold algorithm for different thresholds.

4.3. Estimation of river discharge from satellite radar altimetry

There is no direct space-based method for river discharge estimation. Therefore, it must be calculated from observing hydraulic flow parameters through mathematical formulations or calibrated relationships (rating curves). From Manning's fundamental open channel flow, we can deduce and develop hydraulic relations, which could potentially estimate discharges from space for the so-called ideal river cross-sections (Huang et al., 2019; Sichangi et al., 2016).

Having estimated the precise water level of river from altimetry data, it must be converted into river discharge as the next step. River discharge is functionally related to the water level in a given location. As mentioned above, this relationship is known as the "rating curve" and is determined by simultaneous water level measurements and river discharge, using either simple or complex relationships. The simplest forms of rating curves are observed in stable channels with a constant current. The rating curve usually follows the power-law, but a simple relationship between the water level estimated from the altimetry data (h) and the river discharge (Q) can also be considered (Rantz, 1982). In this study, the following linear function is used to fit the curve.

$$Q_m = a \times h + b \quad (5)$$

$$Q_e = a \times h + b \quad (6)$$

In the above equations, a and b are unknown parameters that must be estimated, Q_m is the in-situ discharges at the river site, and Q_e is the river discharge estimated from the water levels obtained from the altimetry data. First, the unknown coefficients a and b were calculated by fitting the polynomial curve to Q_m , and then Q_e was estimated with the same coefficients. Finally, Q_m and Q_e were compared and evaluated in terms of RMSE, correlation coefficient, and the Nash–Sutcliffe model efficiency coefficient (NSE). It must be mentioned that we examined polynomials of different degrees and among them, according to statistical indicators, the linear function of Eq. (5) and Eq. (6) were selected as the optimal model for our case.

4.4. Estimation of river discharge from satellite images

Estimating river discharge by creating a hydraulic geometric relationship along the cross-section of a channel

is a well known method that many researchers have used (Gleason et al., 2014; Kebede et al., 2020; Leopold & Maddock, 1953; Zhang & Singh, 2006). Therefore, we also used this method, which is a hydraulic relationship between the river width obtained from remote sensing images and the in situ gauge discharge, to estimate the discharge of the Karun River as follows:

$$W = aQ^b \quad (7)$$

where W is the estimated river width from satellite imagery, Q is the in-situ gauge discharge, and a and b are calibrated numerical constants derived from the hydraulic relationship (Eq. 5).

It should be mentioned that the width of the river in our case was available at the location of in-situ station of Karun River. However, to estimate the width of the river at the satellite altimetry footprint across section over the river we used Sentinel 1 and Sentinel 2 missions images and first separated river from its bank via the methods described in Tayfehrostami et al. (2021) and, Tayfehrostami et al. (2022). Next, using SNAP software the width of river at the cross section is extracted from the images of both missions via distance tool of the software.

In this way we developed the time series of the river discharge via Sentinel 1 and Sentinel 2 missions and compared it with measured discharge at in situ station and estimated RMSE, correlation coefficient, relative RMSE, and NSE coefficient of the differences. Finally, the time series of river discharge estimated from altimetry data, SAR images, and optical images were compared with one another. Flowchart of figure 4 gives an overview of our methodology for river discharge monitoring using satellite missions.

As the flowchart of Fig. 4 shows we used satellite altimetry data to derive the water level time series from the re-trackers of the level-2 data, and also re-tracked the returned waveforms of level 1 data of the Sentinel 3B mission by using the threshold algorithm. The resulted water levels were compared with water level of in-situ gauge data and validated. The obtained, precise water level from Sentinel 3B altimetry mission is converted to the river discharge. Moreover, using SAR and optical images we derived the river width and converted it into the river discharge. Finally, the computed discharges were compared with in situ data and validated. In the following sections we will discuss about the results and the validations.

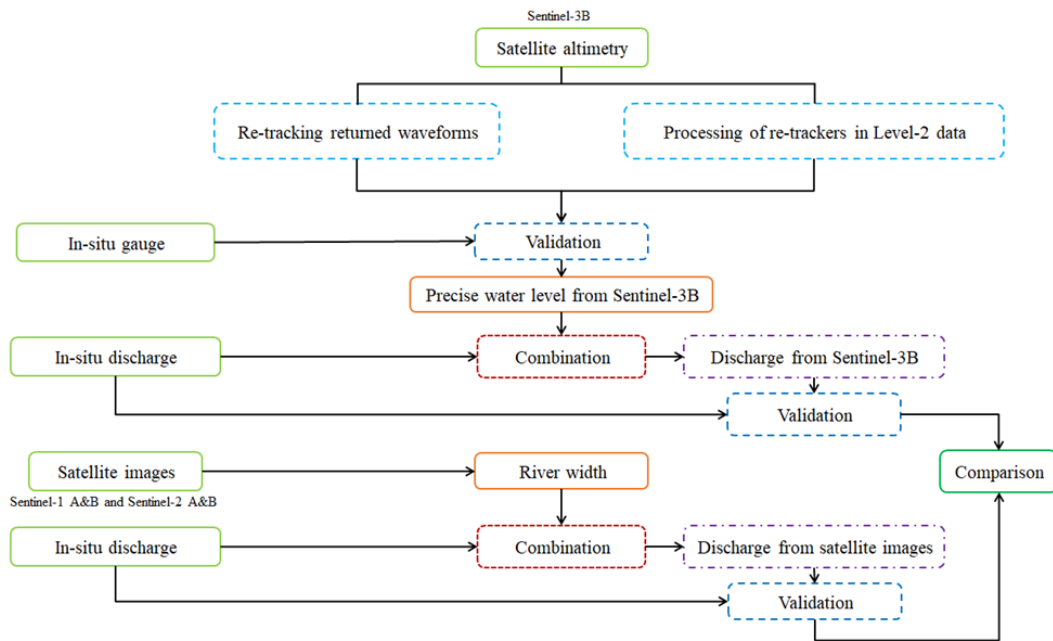


Figure 4. The general flowchart of our methodology for discharge monitoring via satellite radar altimetry and satellite images.

5. Results and discussions

5.1. Evaluation of water level time series

Via discussed analyses we estimated the variations of water level of Karun River from the level-2 and level-1B altimetry data of the Sentinel-3B mission, which are shown in Figures (5 to 9) and Tables (4 to 7). After correcting for

the elevation bias between satellite altimetry and in-situ data due to the difference in elevation datums, the water level time series obtained from the re-trackers in the level-2 data was compared with the in-situ gauge data. The results of this comparison are given in table 4.

Table 4. Summary statistics of the difference between water level obtained from different re-trackers of level-2 data of Sentinel-3B mission and in-situ gauge data of Karun River.

| Level-2 re-trackers | RMSE (m) | Correlation (%) |
|---------------------|----------|-----------------|
| Ocean | 1.71 | 42.77 |
| OCO2 | 1.67 | 47.71 |
| Ice Sheet | 1.75 | 46.29 |
| Sea Ice | 2.04 | 40.42 |
| Tracker Range | 1.57 | 23.04 |

Table (4) shows that the OCO2 re-tracker outperformed other re-trackers in the level-2 data in retrieving the water level of the Karun River. Figure (5) shows the time series of

water level obtained from the re-trackers of the level-2 data. Figures (6 and 7) show the differences and correlations of the time series of water levels obtained from the existing re-trackers with the in-situ gauge water level, respectively.

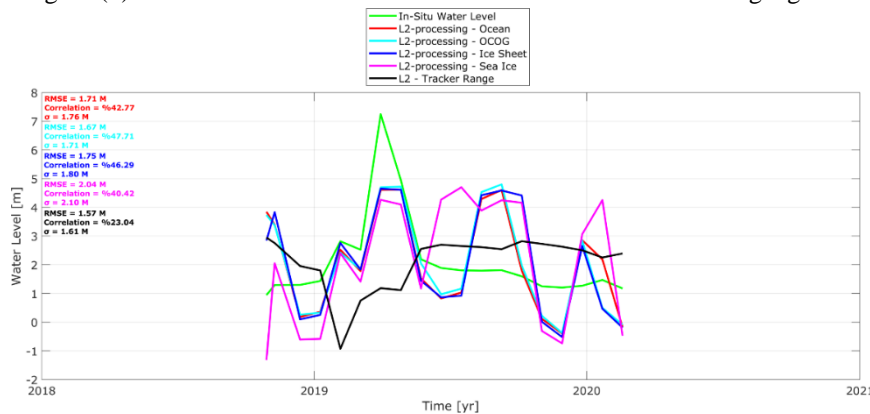


Figure 5. Time series of water levels of Karun River obtained from the re-trackers of level-2 data of the Sentinel-3B (SRAL) mission.

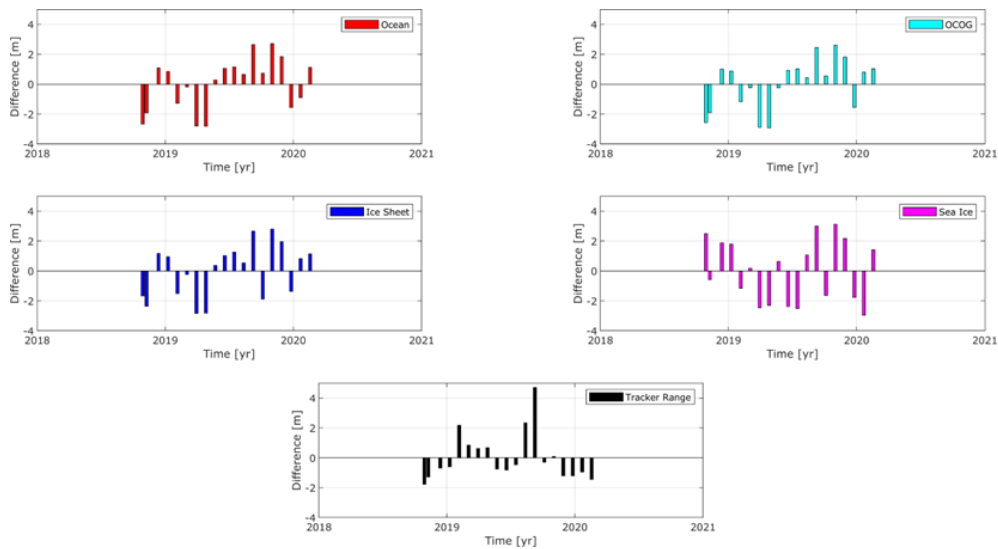


Figure 6. Differences in water levels obtained from re-trackers of level-2 data with Karun River in-situ gauge data.

Figure (6) shows that the OCOG, Ocean, and Ice Sheet re-trackers have the same results in estimating the water level of the Karun River and the difference between these

three re-trackers in the level-2 data with the in-situ gauge water level is almost similar.

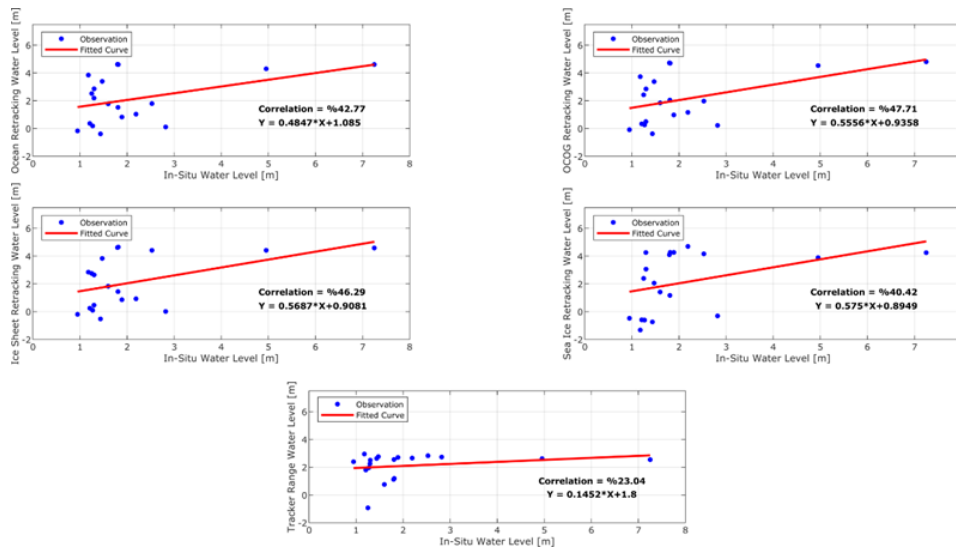


Figure 7. Correlation of water levels obtained from level-2 data with the in-situ gauge water level of Karun River.

Figure 7 re-confirms the close correlation of these three re-trackers with the in-situ gauge data. Next, the water level time series obtained via re-tracking the returned waveforms

based on the threshold algorithm when using different thresholds is compared with the in-situ data. The results of the comparisons are given in Table 5.

Table 5. Summary statistics of differences between water level time series obtained from different thresholds and in-situ gauge data of Karun River.

| Threshold (%) | RMSE (m) | Correlation (%) |
|---------------|----------|-----------------|
| 10 | 2.31 | 12.24 |
| 20 | 2.10 | 24.86 |
| 30 | 2.03 | 32.42 |
| 40 | 1.90 | 37.55 |
| 50 | 1.84 | 41.43 |
| 60 | 1.74 | 46.08 |
| 70 | 1.67 | 48.96 |
| 80 | 1.59 | 52.54 |
| 90 | 1.56 | 53.78 |

From the results shown in the Table 5, it can be seen that the time series of water level obtained from the threshold of 90% results in the smallest RMSE value and the highest

correlation with the in-situ gauge data. The time series of water level obtained from different thresholds are shown in Figure (8).

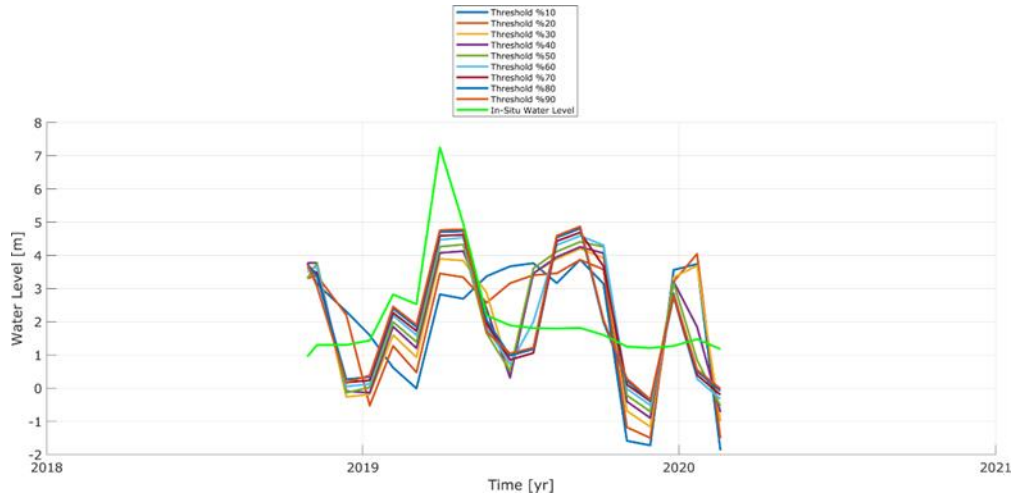


Figure 8. Time series of water levels obtained by different thresholds and the in-situ water level of Karun River.

The best results from re-tracker of level-2 data and the re-tracked waveforms of level-1 data recollected in Table 6 for

easier comparison of the validity of the two optimum satellite derived times series.

Table 6. Evaluation of the final time series of Karun River water level.

| Method | RMSE (m) | Correlation (%) |
|-----------------------------------|----------|-----------------|
| Optimum level-2 re-tracker (OCOg) | 1.67 | 47.71 |
| Optimum threshold (90%) | 1.56 | 53.78 |

Table (6) shows the time series of water level obtained by re-tracking the returned waveforms of Karun River with a threshold of 90%, improves 7.05% the accuracy and increases the correlation with in-situ gauge water level by

12.7%. Therefore, the time series from threshold 90% was selected as the precise water level obtained from satellite altimetry data to estimate the river discharge (Qe).

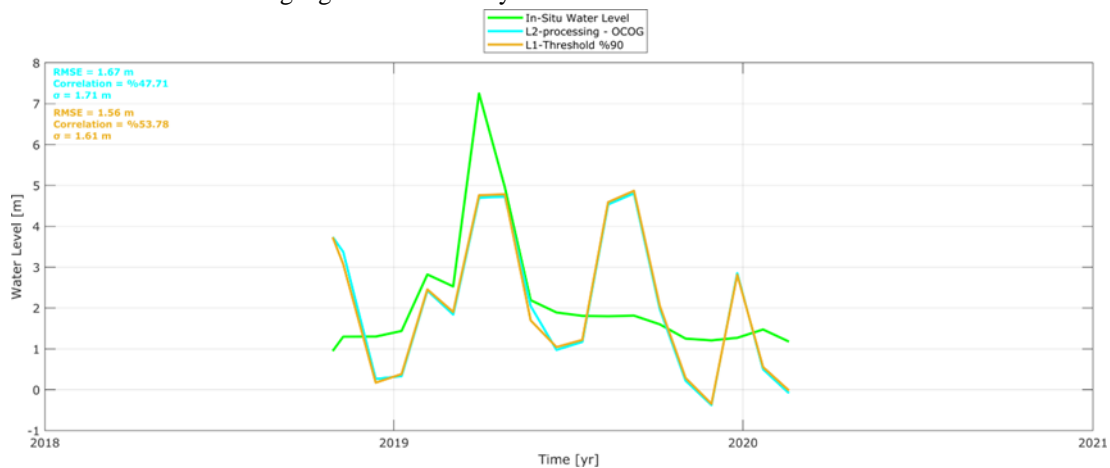


Figure 9. Final time series of Karun River water level.

5.2. Evaluation of river discharge from satellite altimetry

Having obtained the precise water level from the altimetry data of the Sentinel-3B mission, based on the method described in Sect. 4.3, they were converted into river discharge and compared with the in-situ discharge of

the Karun River. Figure 10 shows the time series of river discharge resulting from the precise water level (90% threshold) and in-situ discharge data.

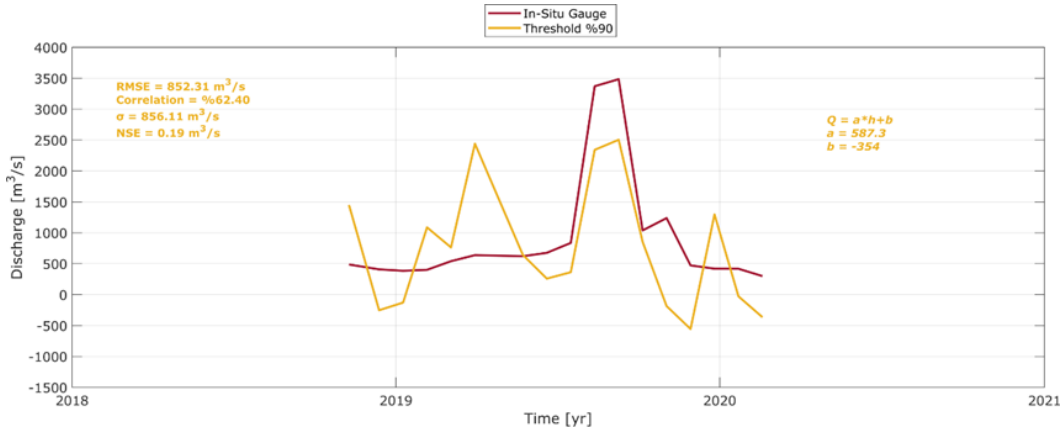


Figure 10. River discharge time series obtained from satellite altimetry data and in-situ discharge of Karun River.

Comparison of two river discharge time series obtained from Sentinel-3B mission altimetry data and in-situ discharge showed the RMSE values of 852/31 m³/s, correlation of 62.40%, and NSE coefficient value of 0.19 m³/s. The above results are influenced by various factors such as the distance of the Sentinel-3B altimetry mission

pass from the in-situ gauge station (Figure 1), the length of the satellite track over the river, the meandering of the Karun River, the vegetation coverage, etc. Figure 11 shows the rating curve obtained from the precise water level from satellite altimetry and in-situ discharge of the Karun River.

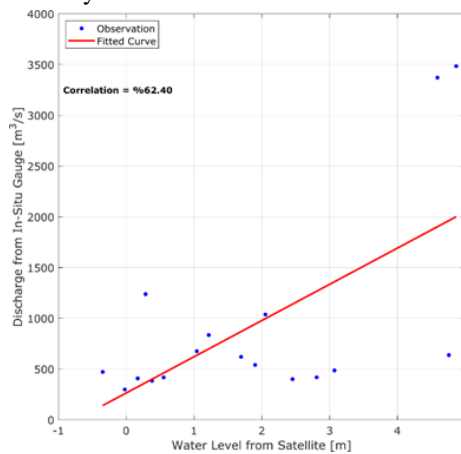


Figure 11. Rating curve obtained from the precise water level from satellite altimetry and in-situ discharge of the Karun River.

5.3. Evaluation of river discharge from satellite images

After estimating the river width from the Sentinel-1 and Sentinel-2 mission images (Figure 12), the estimated river

widths were converted to river discharge by the method described in Sect. 4.4.

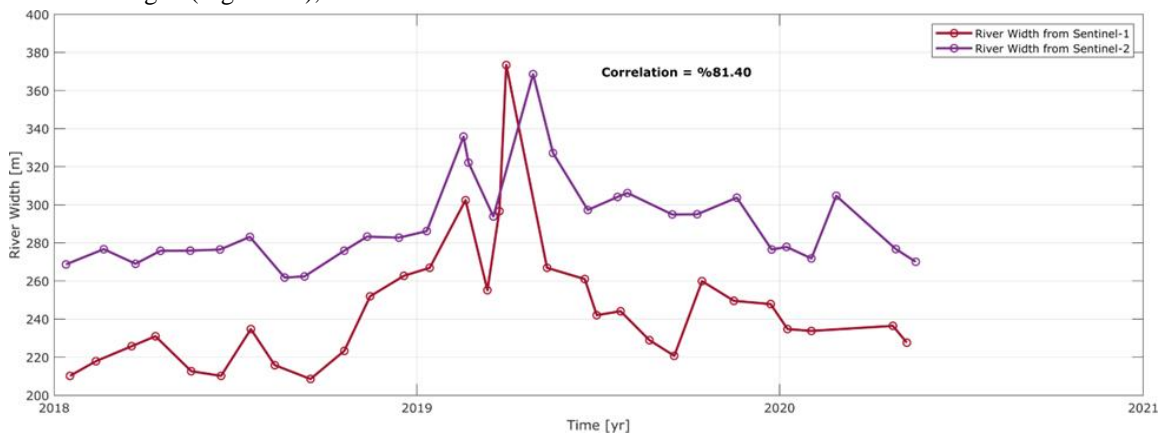


Figure 12. Time series of Karun River width in the cross-section of Ahwaz station from the Sentinel-1 and Sentinel-2 mission images.

As shown in Figure (12), the time series of the estimated river width from the images showed a correlation of 81.40% with each other. Figure (13) shows the river

discharge time series from the Sentinel-1 mission images and in-situ discharges.

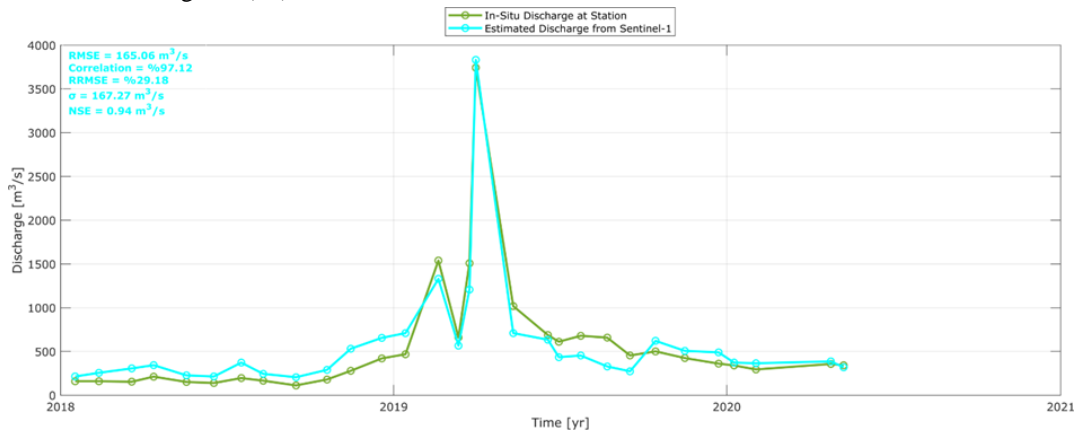


Figure 13. River discharge time series from Sentinel-1 mission images and in-situ discharges of Karun River.

Comparison of two river discharge time series from river width obtained from Sentinel-1 mission images and in-situ discharges of Karun River showed RMSE value of 165.06 m³/s, correlation 97.12%, and NSE coefficient of 0.94 m³/s.

Figure (14) also shows the rating curve obtained from the river width calculated from the Sentinel-1 mission images and the in-situ discharges of the Karun River.

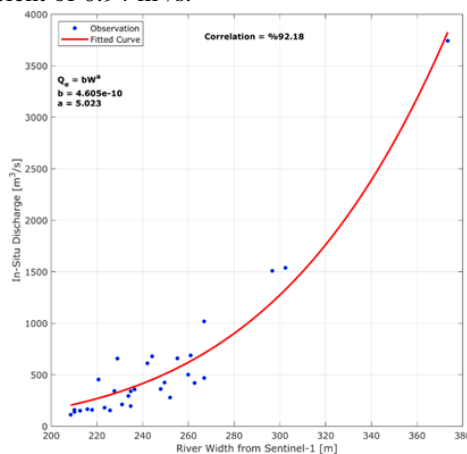


Figure 14. Rating curve from river width of Sentinel-1 images and in-situ discharges of the Karun River.

Similar to the Sentinel-1 mission images, after calculating the river width from the Sentinel-2 mission images, the time series of the river width was converted to the river discharge and compared with the in-situ discharges of the

Karun River. Figure 15 shows the river discharge time series from the Sentinel-2 mission images and in-situ discharges data.

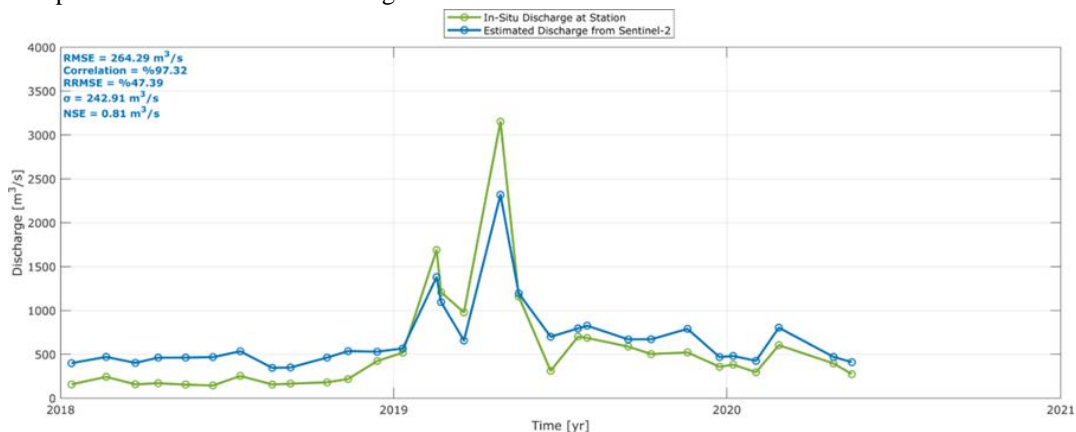


Figure 15. River discharge time series from Sentinel-2 mission images and in-situ discharges data of Karun River.

Comparison of two river discharge time series from river width obtained from Sentinel-2 mission images and in-situ discharges of Karun River showed RMSE value of 264.29 m³/s, correlation of 97.32%, and NSE coefficient of 0.81

m³/s. Figure 16 also shows the rating curve obtained from the river width calculated from the Sentinel-2 mission images and the in-situ discharges of the Karun River.

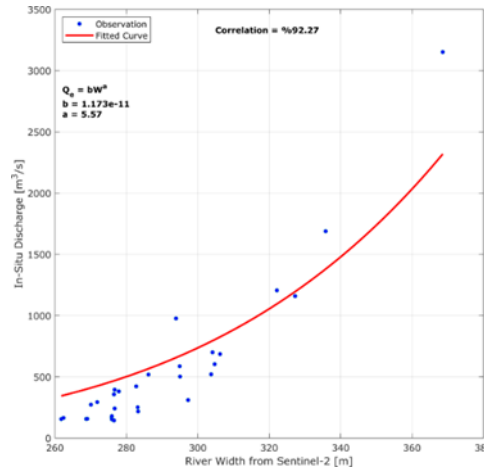


Figure 16. Rating curve from river width of Sentinel-2 images and in-situ discharges of the Karun River.

Finally, the Karun River discharge time series were evaluated and compared from the altimetry data of the

Sentinel-3B mission, the images of the Sentinel-1 mission, and the Sentinel-2 mission, which are shown in Table 7.

Table 7. Summary statistics of comparison of Karun River discharge time series from different satellite missions.

| Method | RMSE (m ³ /s) | Correlation (%) | NSE (m ³ /s) | RRMSE (%) |
|-------------|--------------------------|-----------------|-------------------------|-----------|
| Sentinel-3B | 852.31 | 62.40 | 0.19 | - |
| Sentinel-1 | 165.06 | 97.12 | 0.94 | 29.18 |
| Sentinel-2 | 264.29 | 97.32 | 0.81 | 47.39 |

Table 7 shows that the hydraulic model used to estimate the river discharge from satellite images has high accuracy and good performance. On the other hand, the lower accuracy of river discharge obtained from satellite altimetry data as compared with that of satellite images can be due to various reasons summarized in Sect. 5.2.

6. Conclusions

In this study, using multi missions of Copernicus satellites at the same time period, the discharge of Karun River in Ahwaz province was estimated. Level-1B and Level-2 data of the Sentinel-3B SAR altimeter missions (SRAL) were used to monitor river water level. Furthermore, SAR images of the Sentinel 1 mission and optical images of the Sentinel-2 mission were used to calculate the time series of river width. A threshold algorithm was used to re track the contained returned waveforms of L1B altimetry data over the Karun River. Then, the water levels obtained from the processing of L-2 data and the re-tracking of the returned waveforms with the threshold algorithm compared with the in situ gauge data and the precise water level from Sentinel 3B altimetry data was derived. Finally, by forming a rating curve between the time series of in-situ river discharge, the water level obtained from the Sentinel 3B mission, and the river width

calculated from the remotely sensed images, river discharge was estimated. The results showed that the time series of water level from re-tracking of returned waveforms with threshold algorithm 90% improves 7.05% the accuracy and increases 12.7% correlation with in-situ gauge data as compared with the optimum L-2 water level. It should be noted that monitoring rivers using satellite altimetry is influenced by various factors such as satellite resolution, the way the data is processed, alignment of the satellite track and river relative to each other, the topography around the river, and the size of the radar footprint, along with the complex shape of the river, and the distance between the satellite track and the in-situ gauge station are among the factors that affect the water level estimation. In our case, despite of approximately 11 km distance between the Sentinel-3B mission track and the in-situ gauge station, we arrived at the satisfactory results. Comparison of river discharge time series obtained from Sentinel-3B mission altimetry data and in-situ discharge, resulted the RMSE value of 852/31 m³/s, correlation of 62.40%, and NSE coefficient value of 0.19 m³/s. Furthermore, comparing the time series of river discharge obtained from river width from Sentinel-1 mission images and in-situ discharge showed RMSE values of 165.06 m³/s, the correlation coefficient of 97.12%, and NSE of 0.94 m³/s. On the other hand, a comparison of time series of river discharge obtained from river width calculated from Sentinel-2

mission images and in-situ discharges showed RMSE value of 2626.29 m³/s, correlation of 97.32%, and NSE coefficient of 0.81 m³/s, which indicates the good performance of the hydraulic model used to estimate the river discharges from the river width calculated from satellite images. Finally, we can conclude that various satellite missions of Copernicus are capable to monitor medium and small size rivers and the technique that we used for the Karun River can be applied to other rivers of the country.

Acknowledgments

The authors would like to express their appreciation and thank the Khuzestan Water and Power Authority for providing the in-situ data and information needed for the Karun River. We are also thankful to the European Space Agency (ESA) and the European Organization for the Exploitation of Meteorological Satellites (EUMETSAT) for providing data on the satellite missions used in this study.

References

- Beltaos, S., & Kääb, A. (2014). Estimating river discharge during ice breakup from near-simultaneous satellite imagery. *Cold Regions Science and Technology*, 98, 35–46. <https://doi.org/10.1016/j.coldregions.2013.10.010>
- Biancamaria, S., Bates, P. D., Boone, A., & Mognard, N. M. (2009). Large-scale coupled hydrologic and hydraulic modelling of the Ob river in Siberia. *Journal of Hydrology*, 379(1–2), 136–150. <https://doi.org/10.1016/j.jhydrol.2009.09.054>
- Boehm, J., Kouba, J., & Schuh, H. (2008). Forecast Vienna Mapping Functions 1 for real-time analysis of space geodetic observations. *Journal of Geodesy* 2008 83:5, 83(5), 397–401. <https://doi.org/10.1007/S00190-008-0216-Y>
- Bogning, S., Frappart, F., Blarel, F., Ninõ, F., Mahé, G., Seyler, F., Braun, J. J., Onguéné, R., & Etamé, J. (2018). Estimating river discharges in the ogooué river basin using satellite altimetry data. *International Geoscience and Remote Sensing Symposium (IGARSS)*, 2018-July, 9304–9307. <https://doi.org/10.1109/IGARSS.2018.8519574>
- Calmant, S., & Seyler, F. (2006). Continental surface waters from satellite altimetry. *Comptes Rendus - Geoscience*, 338(14–15), 1113–1122. <https://doi.org/10.1016/j.crte.2006.05.012>
- Cartwright, D. E., & Edden, A. C. (1973). Corrected Tables of Tidal Harmonics. *Geophysical Journal of the Royal Astronomical Society*, 33(3), 253–264. <https://doi.org/10.1111/j.1365-246X.1973.tb03420.x>
- Cazals, C., Rapinel, S., Frison, P. L., Bonis, A., Mercier, G., Mallet, C., Corgne, S., & Rudant, J. P. (2016). Mapping and characterization of hydrological dynamics in a coastal marsh using high temporal resolution Sentinel-1A images. *Remote Sensing*, 8(7). <https://doi.org/10.3390/rs8070570>
- Davis, C. H. (1995). Growth of the Greenland Ice Sheet: A Performance Assessment of Altimeter Retracking Algorithms. *IEEE Transactions on Geoscience and Remote Sensing*, 33(5), 1108–1116. <https://doi.org/10.1109/36.469474>
- Davis, C. H. (1997). A robust threshold retracking algorithm for measuring ice-sheet surface elevation change from satellite radar altimeters. *IEEE Transactions on Geoscience and Remote Sensing*, 35(4), 974–979. <https://doi.org/10.1109/36.602540>
- Deng, X., & Featherstone, W. E. (2006). A coastal retracking system for satellite radar altimeter waveforms: Application to ERS-2 around Australia. *Journal of Geophysical Research: Oceans*, 111(6). <https://doi.org/10.1029/2005JC003039>
- Di Baldassarre, G., & Uhlenbrook, S. (2012). Is the current flood of data enough? A treatise on research needs for the improvement of flood modelling. *Hydrological Processes*, 26(1), 153–158. <https://doi.org/10.1002/hyp.8226>
- Domeneghetti, A., Tarpanelli, A., Brocca, L., Barbetta, S., Moramarco, T., Castellarin, A., & Brath, A. (2014). The use of remote sensing-derived water surface data for hydraulic model calibration. *Remote Sensing of Environment*, 149, 130–141. <https://doi.org/10.1016/j.rse.2014.04.007>
- Drusch, M., Del Bello, U., Carlier, S., Colin, O., Fernandez, V., Gascon, F., Hoersch, B., Isola, C., Laberinti, P., Martimort, P., Meygret, A., Spoto, F., Sy, O., Marchese, F., & Bargellini, P. (2012). Sentinel-2: ESA's Optical High-Resolution Mission for GMES Operational Services. *Remote Sensing of Environment*, 120, 25–36. <https://doi.org/10.1016/j.rse.2011.11.026>
- Emery, C. M., Paris, A., Biancamaria, S., Boone, A., Calmant, S., Garambois, P. A., & Da Silva, J. S. (2018). Large-scale hydrological model river storage and discharge correction using a satellite altimetry-based discharge product. *Hydrology and Earth System Sciences*, 22(4), 2135–2162. <https://doi.org/10.5194/hess-22-2135-2018>
- ESA, Sentinel-3 Altimetry Technical Guide - Sentinel Online. Retrieved August 28, 2021, from <https://sentinel.esa.int/web/sentinel/technical-guides/sentinel-3-altimetry/appendices/faq>
- ESA. (2015). ESA's Optical High-Resolution Mission for GMES Operational Services.
- EUMETSAT. (2017). Sentinel-3 SRAL Marine User Handbook. 38.
- Feng, D., Gleason, C. J., Yang, X., & Pavelsky, T. M. (2019). Comparing Discharge Estimates Made via the

- BAM Algorithm in High- Order Arctic Rivers Derived Solely From Optical CubeSat, Landsat, and Sentinel- 2 Data. *Water Resources Research*, 55(9), 7753–7771. <https://doi.org/10.1029/2019WR025599>
- Frappart, F., Papa, F., Güntner, A., Werth, S., Ramillien, G., Prigent, C., Rossow, W. B., & Bonnet, M. P. (2010). Interannual variations of the terrestrial water storage in the lower ob' basin from a multisatellite approach. *Hydrology and Earth System Sciences*, 14(12), 2443–2453. <https://doi.org/10.5194/hess-14-2443-2010>
- Gao, H. (2015). Satellite remote sensing of large lakes and reservoirs: from elevation and area to storage. *Wiley Interdisciplinary Reviews: Water*, 2(2), 147–157. <https://doi.org/10.1002/wat2.1065>
- Gao, H., Birkett, C., & Lettenmaier, D. P. (2012). Global monitoring of large reservoir storage from satellite remote sensing. *Water Resources Research*, 48(9). <https://doi.org/10.1029/2012WR012063>
- Gao, Q., Makhoul, E., Escorihuela, M. J., Zribi, M., Seguí, P. Q., García, P., & Roca, M. (2019). Analysis of retracker's performances and water level retrieval over the Ebro River basin using sentinel-3. *Remote Sensing*, 11(6), 718. <https://doi.org/10.3390/RS11060718>
- Getirana, A. C. V., & Peters-Lidard, C. (2013). Estimating water discharge from large radar altimetry datasets. *Hydrology and Earth System Sciences*, 17(3), 923–933. <https://doi.org/10.5194/hess-17-923-2013>
- Gleason, C. J., & Hamdan, A. N. (2017). Crossing the (watershed) divide: satellite data and the changing politics of international river basins. *The Geographical Journal*, 183(1), 2–15. <https://doi.org/10.1111/geoj.12155>
- Gleason, C. J., Smith, L. C., & Lee, J. (2014). Retrieval of river discharge solely from satellite imagery and at-many-stations hydraulic geometry: Sensitivity to river form and optimization parameters. *Water Resources Research*, 50(12), 9604–9619. <https://doi.org/10.1002/2014WR016109>
- Gleason, C. J., Wada, Y., & Wang, J. (2018). A Hybrid of Optical Remote Sensing and Hydrological Modeling Improves Water Balance Estimation. *Journal of Advances in Modeling Earth Systems*, 10(1), 2–17. <https://doi.org/10.1002/2017MS000986>
- Hossain, F., Siddique-E-Akbor, A. H., Mazumder, L. C., Shahnewaz, S. M., Biancamaria, S., Lee, H., & Shum, C. K. (2014). Proof of concept of an altimeter-based river forecasting system for transboundary flow inside Bangladesh. *IEEE Journal of Selected Topics in Applied Earth Observations and Remote Sensing*, 7(2), 587–601. <https://doi.org/10.1109/JSTARS.2013.2283402>
- Huang, Q., Li, X., Han, P., Long, D., Zhao, F., & Hou, A. (2019). Validation and application of water levels derived from Sentinel-3A for the Brahmaputra River. *Science China Technological Sciences* 2019 62:10, 62(10), 1760–1772. <https://doi.org/10.1007/S11431-019-9535-3>
- Kebede, M. G., Wang, L., Li, X., & Hu, Z. (2020). Remote sensing-based river discharge estimation for a small river flowing over the high mountain regions of the Tibetan Plateau. *International Journal of Remote Sensing*, 41(9), 3322–3345. <https://doi.org/10.1080/01431161.2019.1701213>
- Kouraev, A. V., Zakharova, E. A., Samain, O., Mognard, N. M., & Cazenave, A. (2004). Ob' river discharge from TOPEX/Poseidon satellite altimetry (1992–2002). *Remote Sensing of Environment*, 93(1–2), 238–245. <https://doi.org/10.1016/j.rse.2004.07.007>
- LeFavour, G., & Alsdorf, D. (2005). Water slope and discharge in the Amazon River estimated using the shuttle radar topography mission digital elevation model. *Geophysical Research Letters*, 32(17), 1–5. <https://doi.org/10.1029/2005GL023836>
- Leopold, L. B., & Maddock, T. J. (1953). The Hydraulic Geometry of Stream Channels and Some Physiographic Implications. In *Geological Survey Professional Paper* 252. <https://doi.org/10.3133/pp252>
- Nagler, T., Rott, H., Ripper, E., Bippus, G., & Hetzenecker, M. (2016). Advancements for Snowmelt Monitoring by Means of Sentinel-1 SAR. *Remote Sensing* 2016, Vol. 8, Page 348, 8(4), 348. <https://doi.org/10.3390/RS8040348>
- Pavlis, N. K., Holmes, S. A., Kenyon, S. C., & Factor, J. K. (2012). The development and evaluation of the Earth Gravitational Model 2008 (EGM2008). *Journal of Geophysical Research: Solid Earth*, 117(B4), 4406. <https://doi.org/10.1029/2011JB008916>
- Rantz, S. E. (1982). Measurement and computation of streamflow: volume 1. Measurement of stage and discharge. In *Water Supply Paper (Vols. 1 & 2)*. <https://doi.org/10.3133/wsp2175>
- Roohi, S. (2017). Performance evaluation of different satellite radar altimetry missions for monitoring inland water bodies. *Geodätisches Institut Der Universität Stuttgart, March*, 173.
- Scharroo, R., & Smith, W. H. F. (2010). A global positioning system - Based climatology for the total electron content in the ionosphere. *Journal of Geophysical Research: Space Physics*, 115(10). <https://doi.org/10.1029/2009JA014719>
- Sichangi, A. W., Wang, L., Yang, K., Chen, D., Wang, Z., Li, X., Zhou, J., Liu, W., & Kuria, D. (2016). Estimating continental river basin discharges using multiple remote sensing data sets. *Remote Sensing of Environment*, 179, 36–53. <https://doi.org/10.1016/j.rse.2016.03.019>

- Smith, L. C., & Pavelsky, T. M. (2008). Estimation of river discharge, propagation speed, and hydraulic geometry from space: Lena River, Siberia. *Water Resources Research*, 44(3). <https://doi.org/10.1029/2007WR006133>
- Sneeuw, N., Lorenz, C., Devaraju, B., Tourian, M. J., Riegger, J., Kunstmann, H., & Bárdossy, A. (2014). Estimating Runoff Using Hydro-Geodetic Approaches. *Surveys in Geophysics*, 35(6), 1333–1359. <https://doi.org/10.1007/s10712-014-9300-4>
- Sulistioadi, Y. B., Tseng, K.-H., Shum, C. K., Hidayat, H., Sumaryono, M., Suhardiman, A., Setiawan, F., & Sunarso, S. (2015). Satellite radar altimetry for monitoring small rivers and lakes in Indonesia. *Hydrol. Earth Syst. Sci*, 19, 341–359. <https://doi.org/10.5194/hess-19-341-2015>
- Sun, W. C., Ishidaira, H., & Bastola, S. (2010). Towards improving river discharge estimation in ungauged basins: Calibration of rainfall-runoff models based on satellite observations of river flow width at basin outlet. *Hydrology and Earth System Sciences*, 14(10), 2011–2022. <https://doi.org/10.5194/hess-14-2011-2010>
- Sun, W., Ishidaira, H., & Bastola, S. (2012). Prospects for calibrating rainfall-runoff models using satellite observations of river hydraulic variables as surrogates for in situ river discharge measurements. *Hydrological Processes*, 26(6), 872–882. <https://doi.org/10.1002/hyp.8301>
- Tang, Q., Gao, H., Lu, H., & Lettenmaier, D. P. (2009). Remote sensing: hydrology. *Progress in Physical Geography: Earth and Environment*, 33(4), 490–509. <https://doi.org/10.1177/0309133309346650>
- Tarpanelli, A., Barbetta, S., Brocca, L., & Moramarco, T. (2013). River Discharge Estimation by Using Altimetry Data and Simplified Flood Routing Modeling. *Remote Sensing*, 5(9), 4145–4162. <https://doi.org/10.3390/rs5094145>
- Tarpanelli, A., Brocca, L., Barbetta, S., Faruolo, M., Lacava, T., & Moramarco, T. (2015). Coupling MODIS and radar altimetry data for discharge estimation in poorly gauged river basins. *IEEE Journal of Selected Topics in Applied Earth Observations and Remote Sensing*, 8(1), 141–148. <https://doi.org/10.1109/JSTARS.2014.2320582>
- Tayfeh Rostami, A., Azmoudeh Ardalan, A., Roohi, S., Pourmina, A. (2021). Retracking Sentinel-3A SAR waveforms to monitor the water level of a small inland water body (Case study: Doroudzan Dam Reservoir, Shiraz, Iran). *Journal of the Earth and Space Physics*, 47(3), 467–483. doi: 10.22059/jesphys.2021.322322.1007311
- Tayfehrostami A, Azmoudeh Ardalan A R, Roohi S, Pourmina A. Dams Surface Area Monitoring from VV and VH Polarization of Sentinel-1 Mission SAR Images (Case study: Doroudzan Dam, Shiraz, Iran). *JGST*. 2021; 10 (4) :103-116 URL: <http://jgst.issge.ir/article-1-988-fa.html>
- Tayfehrostami, A., Azmoudeh Ardalan, A., Pourmina, A., (2022, February). Monitoring the water surface area of Zayandehrud dam lake from SAR and optical remote sensing images. 26th Conference on Surveying & Spatial Information (Geomatics 1400), Iran, Tehran.
- Torres, R., Snoeij, P., Geudtner, D., Bibby, D., Davidson, M., Attema, E., Potin, P., Rommen, B. Ö., Floury, N., Brown, M., Traver, I. N., Deghaye, P., Duesmann, B., Rosich, B., Miranda, N., Bruno, C., L'Abbate, M., Croci, R., Pietropaolo, A., ... Rostan, F. (2012). GMES Sentinel-1 mission. *Remote Sensing of Environment*, 120, 9–24. <https://doi.org/10.1016/j.rse.2011.05.028>
- Tourian, M. J., Schwatke, C., & Sneeuw, N. (2017). River discharge estimation at daily resolution from satellite altimetry over an entire river basin. *Journal of Hydrology*, 546, 230–247. <https://doi.org/10.1016/j.jhydrol.2017.01.009>
- Tourian, M. J., Sneeuw, N., & Bárdossy, A. (2013). A quantile function approach to discharge estimation from satellite altimetry (ENVISAT). *Water Resources Research*, 49(7), 4174–4186. <https://doi.org/10.1002/wrcr.20348>
- Wahr, J. M. (1985). Deformation induced by polar motion. *Journal of Geophysical Research*, 90(B11), 9363–9368. <https://doi.org/10.1029/JB090iB11p09363>
- Wang, L., Sichangi, A. W., Zeng, T., Li, X., Hu, Z., & Genanu, M. (2019). New methods designed to estimate the daily discharges of rivers in the Tibetan Plateau. In *Science Bulletin* (Vol. 64, Issue 7, pp. 418–421). Elsevier B.V. <https://doi.org/10.1016/j.scib.2019.03.015>
- Zakharova, E. A., Kouraev, A. V., Cazenave, A., & Seyler, F. (2006). Amazon River discharge estimated from TOPEX/Poseidon altimetry. *Comptes Rendus Geoscience*, 338(3), 188–196. <https://doi.org/10.1016/j.crte.2005.10.003>
- Zhang, L., & Singh, V. P. (2006). Bivariate Flood Frequency Analysis Using the Copula Method. *Journal of Hydrologic Engineering*, 11(2), 150–164. [https://doi.org/10.1061/\(asce\)1084-0699\(2006\)11:2\(150](https://doi.org/10.1061/(asce)1084-0699(2006)11:2(150)